Chinese Journal of Natural Medicines

Potassium dehydroandrographolide succinate regulates the *MyD88/CDH13* signaling pathway to enhance vascular injury-induced pathological vascular remodeling

Qiru GUO, Jiali LI, Zheng WANG, Xiao WU, Zhong JIN, Song ZHU, Hongfei LI, Delai ZHANG, Wangming HU, Huan XU, Lan YANG, Liangqin SHI, Yong WANG

Citation: Qiru GUO, Jiali LI, Zheng WANG, Xiao WU, Zhong JIN, Song ZHU, Hongfei LI, Delai ZHANG, Wangming HU, Huan XU, Lan YANG, Liangqin SHI, Yong WANG, Potassium dehydroandrographolide succinate regulates the *MyD88/CDH13* signaling pathway to enhance vascular injury-induced pathological vascular remodeling, Chinese Journal of Natural Medicines, 2024, 22(1), 62-74. doi: 10.1016/S1875-5364(24)60562-5.

View online: https://doi.org/10.1016/S1875-5364(24)60562-5

Available online at www.sciencedirect.com
ScienceDirect
Chinese Journal of Natural Medicines 2024, **22**(1): 62-74
doi: 10.1016/S1875-5364(24)60562-5
Chinese Journal of Natural Medicines

•Original article•

Potassium dehydroandrographolide succinate regulates the *MyD88/CDH13* signaling pathway to enhance vascular injury-induced pathological vascular remodeling

GUO Qiru[1Δ], LI Jiali[1Δ], WANG Zheng[1Δ], WU Xiao[1Δ], JIN Zhong[1], ZHU Song[2], LI Hongfei[1], ZHANG Delai[2], HU Wangming[1], XU Huan[1], YANG Lan[1], SHI Liangqin[1], WANG Yong[1*]

[1] *College of Basic Medicine, Chengdu University of Traditional Chinese Medicine, Chengdu 610000, China;*
[2] *Chengdu University of Traditional Chinese Medicine, Hospital of Chengdu University of Traditional Chinese Medicine, Chengdu 610000, China*

Available online 20 Jan., 2024

[ABSTRACT] Pathological vascular remodeling is a hallmark of various vascular diseases. Previous research has established the significance of andrographolide in maintaining gastric vascular homeostasis and its pivotal role in modulating endothelial barrier dysfunction, which leads to pathological vascular remodeling. Potassium dehydroandrographolide succinate (PDA), a derivative of andrographolide, has been clinically utilized in the treatment of inflammatory diseases precipitated by viral infections. This study investigates the potential of PDA in regulating pathological vascular remodeling. The effect of PDA on vascular remodeling was assessed through the complete ligation of the carotid artery in C57BL/6 mice. Experimental approaches, including rat aortic primary smooth muscle cell culture, flow cytometry, bromodeoxyuridine (BrdU) incorporation assay, Boyden chamber cell migration assay, spheroid sprouting assay, and Matrigel-based tube formation assay, were employed to evaluate the influence of PDA on the proliferation and motility of smooth muscle cells (SMCs). Molecular docking simulations and co-immunoprecipitation assays were conducted to examine protein interactions. The results revealed that PDA exacerbates vascular injury-induced pathological remodeling, as evidenced by enhanced neointima formation. PDA treatment significantly increased the proliferation and migration of SMCs. Further mechanistic studies disclosed that PDA upregulated myeloid differentiation factor 88 (*MyD88*) expression in SMCs and interacted with T-cadherin (*CDH13*). This interaction augmented proliferation, migration, and extracellular matrix deposition, culminating in pathological vascular remodeling. Our findings underscore the critical role of PDA in the regulation of pathological vascular remodeling, mediated through the *MyD88*/*CDH13* signaling pathway.

[KEY WORDS] Potassium dehydroandrographolide succinate; Smooth muscle cell; Myeloid differentiation factor 88; T-cadherin; Pathological vascular remodeling

[CLC Number] R965 **[Document code]** A **[Article ID]** 2095-6975(2024)01-0062-13

Introduction

Pathological vascular remodeling plays a pivotal role in the progression of serious cardiovascular diseases [1], including pulmonary arterial hypertension, atherosclerosis, aneurysm, vascular stiffness, restenosis after angioplasties, varicose veins, and vascular calcification.

The clinical prevention and treatment of vascular diseases present ongoing challenges. A variety of surgically-based treatments have been developed to address a broad spectrum of vascular disorders. Specifically, treatment modalities for carotid artery stenosis encompass carotid endarterectomy (CEA), carotid artery stenting (CAS), and transcarotid artery revascularization (TCAR). Additionally, aneurysm management strategies have evolved to include the replacement with synthetic aortic grafts and endovascular aneurysm repair [2, 3]. While these strategies primarily target symptomatic relief, they may inadvertently exacerbate the underlying damage to the vascular wall.

[Received on] 23-Jul.-2023
[Research funding] This study was supported by the National Natural Science Foundation of China (Nos. 81741007 and 81870363); the Science & Technology Departments of Sichuan Province (No. 2020JDTD0025); the Grant from Chengdu University of Traditional Chinese Medicine (Nos. 008066, 030038199, BJRC2018001/030041023, 030041224, ZKYY2004/030055180 and 242030016).
[*]**Corresponding author]** E-mail: wangyong@cdutcm.edu.cn
[Δ]These authors contributed equally to this work.
These authors have no conflict of interest to declare.

The majority of vascular diseases are triggered by endothelial cell dysfunction, leading to smooth muscle cells (SMCs) phenotypic switching and extracellular matrix disorganization [4-8]. The vascular endothelium, comprising a monolayer of endothelial cells, forms the inner lining of blood vessels. Various stressors, such as oxidative stress, reactive oxygen species [9], impaired synthesis and release of endothelial-dependent vasodilatory and vasoconstrictive factors [10], disturbed shear stress [11], metabolic disorders [12], and aging [13], contribute to endothelial dysfunction. This dysfunction is characterized by reduced vasodilation, a proinflammatory state, and prothrombotic properties, playing a crucial role in the development of atherosclerosis, cancer-related angiogenesis, and vascular inflammation associated with vascular leakage and infectious diseases [4].

The vascular endothelium induces SMC relaxation through nitric oxide (NO)-mediated cyclic guanosine monophosphate (cGMP) production, SMC hyperpolarization predominantly regulated by hydrogen peroxide (H_2O_2), and SMC contraction [14]. Endothelial dysfunction is also associated with SMC phenotypic changes leading to pathological remodeling, such as vascular stiffness and restenosis post-angioplasty [15].

MyD88, initially identified as a myeloid differentiation marker, plays a critical role in regulating the innate immune response [16-18]. Inhibition of *MyD88* reduces neointima formation in response to vascular injury [19-21]. *MyD88* deficiency in leukocytes dramatically suppresses AngII-induced AAAs and atherosclerosis [22]. However, the role of *MyD88*-associated signaling pathways in regulating pathological vascular remodeling remains poorly understood.

CDH13, a unique member of the cadherin superfamily, is glycosylphosphatidylinositol-anchored and expressed in endothelial and medial smooth muscle cells. It is essential for maintaining normal vascular architecture [23-25]. *CDH13* is abundantly expressed in vascular endothelial cells and SMCs within atherosclerotic regions, restenosis, and tumor-penetrating blood vessels [26-28]. While *CDH13* expression promotes tumor vascularization and enhances tumor growth [29, 30], it enhances autophagy in SMCs under growth factor deprivation [31]. Some studies have indicated that *CDH13* suppresses pathological angiogenesis specifically by targeting endothelial cell migration and suppresses vascular neointima formation induced by carotid artery ligation [32, 33]. However, the contribution of *CDH13*-associated signaling pathways to pathological vascular remodeling is not fully elucidated.

Our previous studies have demonstrated the critical role of andrographolide in maintaining gastric vascular homeostasis and regulating pathological vascular remodeling [34, 35]. Potassium dehydroandrographolide succinate (PDA), a derivative of andrographolide produced through esterification, is chemically named 14-11,12-didehydroandrographolide 19-bissuccinate mono-potassium salt. PDA has been clinically employed in the therapeutic treatment of inflammatory diseases induced by virus infection [36]. We observed that PDA is critical in regulating the vascular endothelium barrier. This study aimed to determine whether PDA regulates SMC-associated pathological vascular remodeling and study the underlying mechanism.

Material and Methods

Animal ethical approval

Animals used in this study received ethical approval from the Experimental Animal Ethics Committee of Chengdu University of Traditional Chinese Medicine (Ethical Approval Number: 2019-04). The 3-week-old male C57/BL6 mice (Charles River Laboratories, Beijing, China) were raised under a specific pathogen-free (SPF) environment. After one week of acclimatization, until the mice reached an average weight of 20 g, they were randomly divided into two groups.

Complete ligation model of mouse left common carotid artery

The mouse model employed to induce vascular remodeling through complete ligation of the left common carotid artery was based on a previously established protocol. Briefly, mice were subjected to a pretreatment regimen with PDA (20 $mg \cdot kg^{-1}$) for five consecutive days. Subsequently, they were anesthetized using a combination of ketamine (80 $mg \cdot kg^{-1}$) and xylazine (5 $mg \cdot kg^{-1}$) by intraperitoneal injection. The left common carotid arteries were then surgically exposed and completely ligated at the bifurcation site. Tissue samples were harvested following continuous treatment with PDA for either 14 or 21 days. Sections (5 μm) were collected between 100 and 1000 μm from the ligation site, and morphological analysis was conducted using hematoxylin and eosin (H&E) staining. The quantification of neointima areas and media layer areas using Image J software.

Rat aortic SMC culture

The culture of SMCs)from the thoracic artery of Sprague-Dawley rats was carried out *as per* the protocol outlined in a previous report. Initially, the thoracic aorta was harvested from anesthetized Sprague-Dawley rats. Under a microscope, periadventitial tissues were carefully removed, and the endothelium was denuded. The aorta was then subjected to digestion using Blend Enzyme III solution (Roche, 0.5 $U \cdot mL^{-1}$) for 10 min at 37 °C to facilitate the removal of the adventitial layer. Subsequently, the medial layer of the aorta was minced into small pieces. These pieces underwent a second digestion with Blend Enzyme III for 2 hours at 37 °C. Following digestion, the cells were suspended in Dulbecco's Modified Eagle Medium (DMEM) supplemented with 10% Fetal Bovine Serum (FBS).

Cell Counting Kit-8 (CCK-8) cell proliferation assay

A total of 3×10^3 rat SMCs (each well) were seeded in 96-well culture plates. These cells were then exposed to PDA 10 $\mu mol \cdot L^{-1}$ for 24 h. Post-treatment, cell proliferation was quantitatively measured by determining the absorbance at 450 nm utilizing CCK-8.

Bromodeoxyuridine (BrdU) incorporation assay

Rat aortic SMCs were incubated in a culture medium

supplemented with PDA (10 μmol·L^{-1}). Subsequent to this treatment, the cells were labeled with BrdU for 24 h. The integration of BrdU into proliferating SMCs was then assessed through immunofluorescence staining, enabling the evaluation of cell proliferation.

Boyden chamber migration assay

In this assay, 1 × 10^6 SMCs were suspended in 100 μL of serum-free culture medium and subsequently seeded into a Boyden chamber (Falcon). The chamber was positioned in a 24-well culture plate containing 500 μL of complete culture medium, enriched with 10% FBS and 10 μmol·L^{-1} PDA. Following incubation, cell migration was ascertained by staining the migrated cells with crystal violet, and their enumeration was performed to quantify the migratory capacity of the SMCs.

Spheroid sprouting assay

The spheroid sprouting assay was performed in accordance with the previously established method. Initially, a methylcellulose solution was prepared by dissolving 6 g of methylcellulose (Sigma) in 250 mL of pre-warmed serum-free medium, to which an equal volume (250 mL) of DMEM containing 10% serum was added. Cells were suspended in the methylcellulose solution, formulated by combining 10 mL of the methylcellulose solution with 40 mL of culture medium to facilitate sphere formation. Subsequently, a neutralized collagen solution was dispensed into a 24-well culture plate and incubated at 37 °C until the collagen solidified. The cell-containing spheres were then mixed with additional dissolved collagen solution and transferred onto the solidified collagen layer in the culture plate. This assembly was further solidified by incubating the culture plate for 30 min at 37 °C. Following this, 200 μL of complete medium enriched with PDA was added, and the cultures were incubated overnight. Spheroid sprouting was visualized post-calcein AM staining. Imaging was performed using a confocal microscope (Leica Microsystem CMS GmbH). Quantitative analysis of sprouting, including the enumeration of sprouts and measurement of sprout length for each sphere, was conducted using Image J software.

H&E staining, immunohistochemistry (IHC), and immunofluorescence staining (IF)

For histological and immunohistochemical analyses, carotid arteries were harvested and fixed in 4% paraformaldehyde overnight at 4 °C. The tissues were then embedded in paraffin, and 5 μm thick sections were prepared. H&E staining was conducted following the protocol established in our previous study [37]. For IHC staining, the tissue sections were deparaffinized and subjected to antigen retrieval using citric acid for 5 to 10 min. After antigenic unmasking, the sections were incubated with *MyD88* (Affinity), *CDH13* (Pro Sci), and *SM-α-actin* (Santa Cruz) overnight at 4 °C, followed by incubation with biotinylated secondary antibody (Vector Laboratories) for 1 h at room temperature and then with the avidin-biotin complex (ABC) solution (Vector Laboratories) for 30 min at room temperature. The targets were visualized after the DAB solution was added. For IF staining, the deparaffinized tissue sections were permeabilized with PBS containing 0.25% Triton-X-100 and blocked with 10% goat serum. The sections were then incubated with primary antibodies overnight at 4 °C, followed by incubation with Alexa Fluor 594-conjugated or Alexa Fluor 488-conjugated secondary antibodies for 1 h at room temperature. Nuclei were counterstained with 4′,6-diamidino-2-phenylindole (DAPI). For BrdU staining, DNA was denatured using 2 mol·L^{-1} HCl before antibody incubation. Finally, images were captured using confocal microscopy (LS510, Zeiss).

Protein extraction and western blotting

For protein analysis, rat SMCs were lysed using RIPA buffer to extract proteins. The protein concentration was quantified using a BCA Protein Assay Kit (Biosharp). The proteins were denatured at 98 °C and subsequently separated by sodium dodecyl sulfate-polyacrylamide gel electrophoresis (SDS-PAGE). Following electrophoresis, the proteins were transferred onto polyvinylidene fluoride (PVDF) membranes. The membranes were blocked using 5% fat-free milk and then incubated with specific primary antibodies at 4 °C overnight. After appropriate washing and incubation with secondary antibodies, the protein bands were visualized using an ImageQuan LAS4000 Image Station. The density of the protein bands was quantified using Imagequant TL software, facilitating the analysis of protein expression levels.

Real-time polymerase chain reaction (PCR) analysis

Total RNA was isolated from rat SMCs utilizing the TRIzol reagent. The concentration and purity of RNA were ascertained using a spectrophotometer (Denovix, USA). For cDNA synthesis, 600 ng of RNA served as the template. Random hexamer primers were employed in the reverse transcription reaction using the iScript cDNA Synthesis Kit. Quantitative real-time PCR (qPCR) was conducted in duplicates for each sample using the Bio-Rad Real-Time PCR System. The specific primer sequences utilized in this study are detailed in the provided primer list table. Relative gene expression levels were calculated using the $2^{-\Delta\Delta Ct}$ method, with *RPLP0* serving as the reference gene for the normalization of expression levels.

Molecular docking simulation of PDA with MyD88 and CDH13

A molecular docking simulation was performed to evaluate the binding energy of PDA with *MyD88* and *CDH13* using Autodock Vina 1.5.6 software, which was developed by Olson's research group. The three-dimensional structures of *MyD88* and *CDH13* were retrieved from the RCSBPDB database (http://www.rcsb.org/). A binding energy value less than zero was indicative of spontaneous binding, suggesting a natural propensity for interaction between the molecules. Furthermore, the lower the binding energy, the more stable the resulting molecular conformation.

Co-immunoprecipitation assay

For the co-immunoprecipitation assay, total protein was

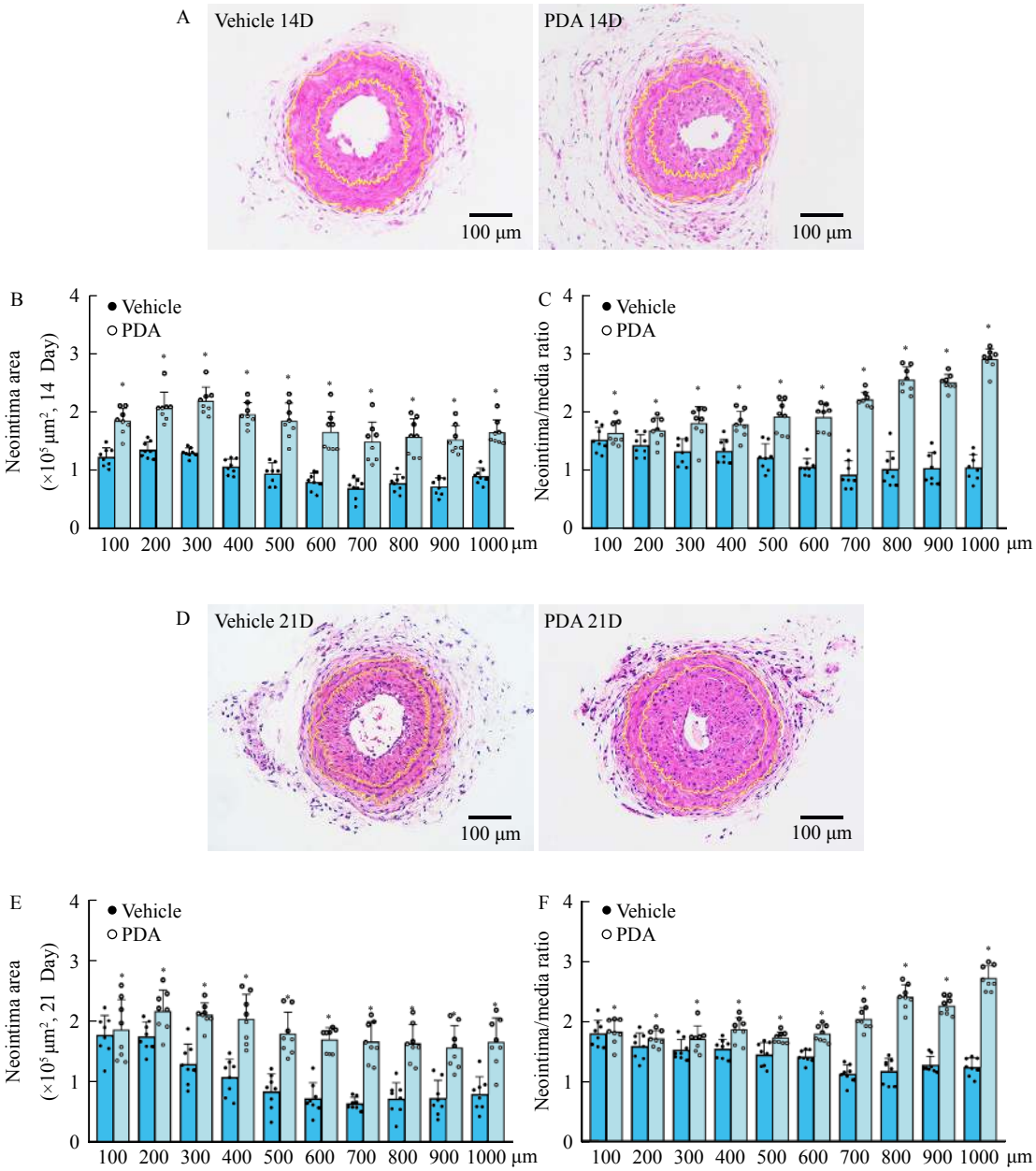

Fig. 1 PDA enhances vascular injury-induced neointima formation. (A) C57BL/6 mice were subjected to complete ligation of the left common carotid artery and treated with intraperitoneal injection of PDA (20 mg·kg^{-1}) for 14 days. Arteries were harvested and embedded in paraffin. Slides of 5 μm thickness were collected from various parts of the ligation site. H&E staining was used to observe the morphological changes of blood vessels. (B, C) Analysis of the area of neointimal hyperplasia and the ratio of neointima area to media area (n = 8). (D) PDA (20 mg·kg^{-1}) was injected intraperitoneally for 21 days and is a representative image of H&E staining. (E, F) Analysis of the area of neointimal hyperplasia and the ratio of neointima area to media area (n = 8). Data are expressed as mean ± SEM. $^{*}P < 0.05$ *vs* Vehicle group.

extracted from SMCs using RIPA buffer to obtain a clear cell lysate. This lysate was initially precleared with anti-species-specific IgG beads to reduce non-specific binding. Subsequently, the precleared lysate was incubated with specific antibodies against *MyD88* (sourced from Affinity) and *CDH13* (sourced from Pro Sci). Following the antibody incubation, the lysate was further incubated with pre-equilibrated protein A/G agarose beads. The co-immunoprecipitated targets were then analyzed using Western blotting.

Statistical analysis

Quantitative data are presented as the mean ± standard error of the mean (SEM). Statistical analyses were performed using GraphPad Prism software. The normality of data distribution was assessed using the Kolmogorov-Smirnov test. For statistical comparisons between the two groups, a two-tailed unpaired Student's *t*-test was employed. When multiple comparisons were required, one- or two-way analysis of variance (ANOVA) was conducted, followed by Bonferroni's post hoc

tests as appropriate. *P*-values were calculated on a two-sided basis, with a threshold of $^{*}P < 0.05$ set for statistical significance.

Results

PDA enhances vascular injury-induced neointima formation

To investigate whether PDA is involved in regulating pathological vascular remodeling, we established a vascular injury model in C57BL/6 mice through the complete ligation of the left common carotid artery. Animals were pretreated with PDA (20 mg·kg^{-1}) for seven consecutive days by intraperitoneal injection, with treatment continued until tissue harvesting. H&E staining was performed to assess vascular morphological alterations. After 14 consecutive days of treatment, a marked induction of neointimal formation was observed (Fig. 1A). We analyzed the lumen, neointima, and media areas and observed that PDA treatment did not change the media area (Supplementary Fig. S1A and S1B). However, it led to an increase in the area of neointimal hyperplasia and the ratio of neointima to media areas, accompanied by a decrease in the lumen area (Figs. 1B and 1C). Furthermore, arterial samples were also collected 21 days post-surgery. Neointima areas at varying distances (100−1000 μm) from the ligation site were analyzed using Image J software based on H&E staining. The results showed a substantial increase in neointimal areas following PDA treatment (Fig. 1D). While no statistical changes in the SMC layer of media were noted, there was a significant increase in the neointima areas and the ratio of neointima to media areas, along with a reduction in lumen areas (Figs. 1E and 1F; Supplementary Figs. S2A and S2B). These findings collectively suggest that PDA induces neointima formation following vascular injury.

PDA promotes the proliferation of vascular SMCs

SMC phenotypic switching, from a differentiated to a dedifferentiated state, is marked by increased proliferation and migration, contributing to various vascular diseases. We sought to determine whether PDA enhances SMC proliferation. Initial assays using varying doses of PDA (1, 5, 10, and 20 μmol·L^{-1}) showed no significant impact on SMC viability, as assessed by the CCK-8 assay (Supplementary Fig. S3). However, subsequent analysis revealed that PDA treatment notably enhanced the proliferation of SMCs. Rat aortic SMCs treated with PDA (10 μmol·L^{-1}) demonstrated a significant increase in cell numbers after 24-, 48-, and 72-h treatment (Fig. 2A). Meanwhile, PDA treatment facilitated the entry of SMCs into the synthesis phase of the cell cycle, as determined by flow cytometry following PI staining (Fig. 2B; Supplementary Fig. S4). Real-time PCR analysis was conducted to assess the expression of cell growth-related genes post-PDA treatment. The results revealed that PDA upregulated genes associated with the positive regulation of the cell cycle, including *Cav1*, *CCN3*, *Id2*, *Ddx39B*, and *FGF2* (Fig. 2C). Furthermore, the BrdU incorporation assay indicated an increase in BrdU-positive SMCs following PDA treatment, as identified through immunofluorescence staining (Figs. 3D and 3E). IHC staining of *PCNA* and *Ki67* was also performed to validate whether PDA promotes SMC proliferation in our animal model. In the common carotid artery ligation model, PDA treatment markedly increased the number of *PCNA*- and *Ki67*-positive SMCs within the neointima (Figs. 3F and 3G; Supplementary Figs. S5A and S5B). Additionally, in a skeletal muscle injury-induced angiogenesis model, PDA treatment was observed to elevate *PCNA* expression, as verified by IF staining. IHC staining further corroborated that PDA treatment significantly raised the number of *PCNA*- and *Ki67*-positive SMCs in newly formed vessels (Figs. 2H and 2I; Supplementary Figs. S6A−S6C, S7A−S7C). These data indicate that PDA promotes the proliferation of vascular SMCs.

PDA promotes the migration of rat SMCs

To determine the influence of PDA on the migratory behavior of rat SMCs, a key event during SMC phenotypic switching, we conducted real-time PCR to evaluate the expression of the extracellular matrix-related genes. The results revealed that PDA treatment markedly reduced the transcription levels of *Col3a1*, *Has2*, *Versican*, and *MMP9* (Supplementary Fig. S8). Additionally, the Boyden chamber migration assay was employed to directly observe the migratory capacity of SMCs in the presence of PDA. The results showed a significant increase in the number of SMCs migrating through the chamber in response to PDA treatment (Figs. 3A and 3B). Furthermore, the spheroid sprouting assay was performed to provide additional insights into the migratory behavior of SMCs under PDA treatment. This assay revealed that PDA notably enhanced both the number and length of sprouts from SMC spheroids (Figs. 3C−3E). Collectively, these findings demonstrate that PDA significantly promotes the migration of rat SMCs.

PDA induces SMCs MyD88 expression following vascular injury stimulation

The molecular mechanisms underlying the phenotypic switching of SMCs, characterized by enhanced proliferation and migration following treatment with PDA, were investigated in this study. Initial investigations involved treating rat SMCs with PDA and analyzing various signaling pathways using real-time PCR. A significant increase in the transcription levels of *MyD88* and *CDH13* was noted post-PDA treatment (Supplementary Fig. S9). Subsequent experiments were aimed at understanding the specific influence of PDA on *MyD88* expression. Real-time PCR analysis showed a considerable induction in *MyD88* transcription levels following PDA treatment (Fig. 4A). Further, SMCs were exposed to varying concentrations of PDA (1, 5, 10, 15, and 20 μmol·L^{-1}), and protein levels were assessed through the Western blotting assay. The results indicated that PDA concentrations ranging from 1 to 20 μmol·L^{-1} significantly elevated MyD88 protein levels, with the highest expression observed at 5, 10, and 15 μmol·L^{-1} PDA treatment (Figs. 4B and 4C). Our Western blotting results revealed that SMCs treated with 10 μmol·L^{-1} PDA demonstrated an elevated ex-

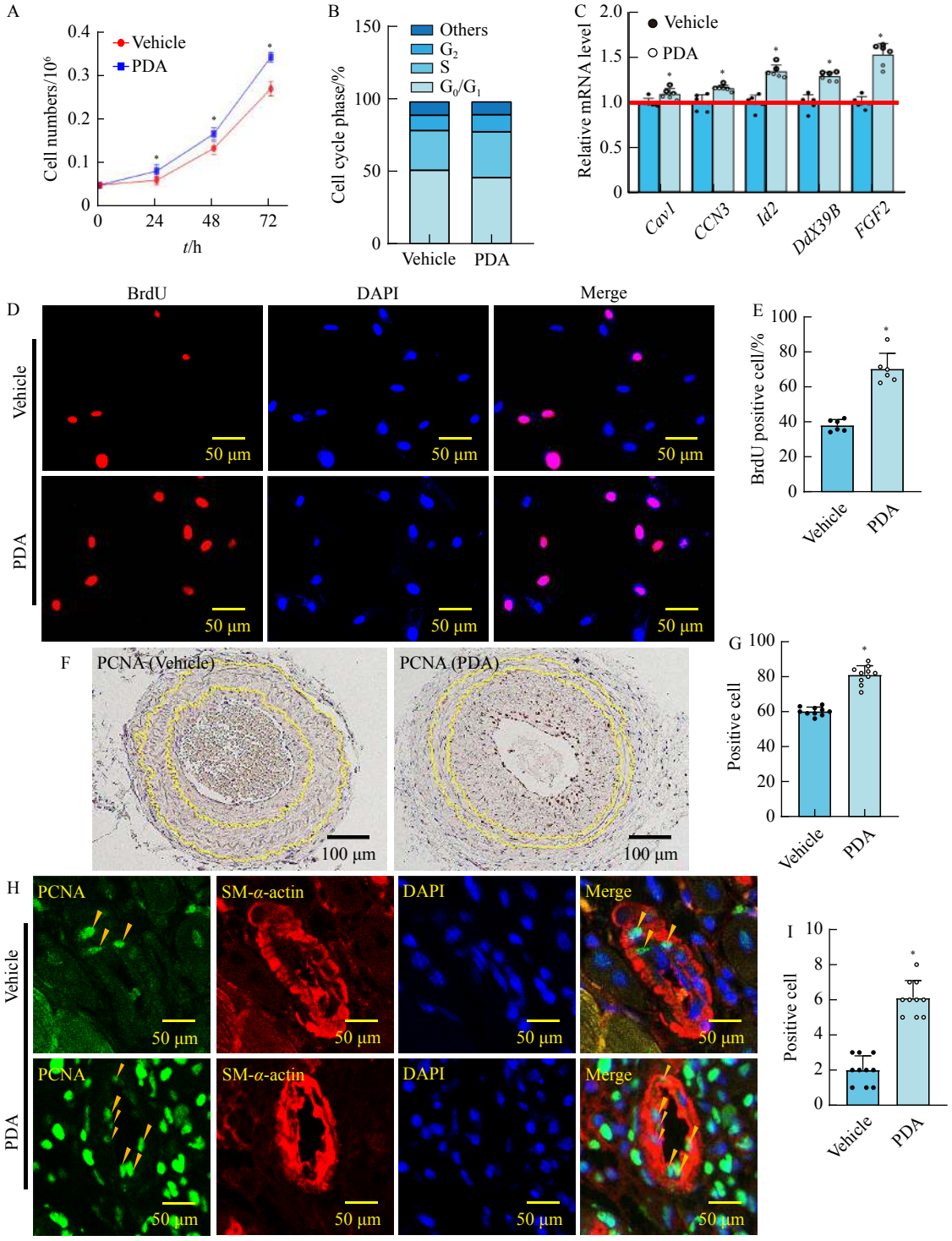

Fig. 2 PDA promotes the proliferation of vascular SMCs. (A) SMCs of rats were treated with PDA (10 μmol·L^{-1}), and the number of cells at different time points was calculated (n = 6). (B) SMCs were treated with PDA (10 μmol·L^{-1}), stained with propidium iodide (PI), and analyzed for cell cycle by flow cytometry. (C) Detection of the mRNA levels of proliferation-related genes *via* real-time PCR (n = 6). (D) Rat SMCs were incubated with BrdU labeling buffer for 20 h, followed by PDA treatment overnight. BrdU incorporation and BrdU-positive cells were detected by IF staining, and the results are shown in (E). (F) The proliferation marker gene *PCNA* in the left common carotid artery ligation model was stained by IHC staining. *PCNA*-positive SMCs in neointima areas are shown in (G) (n = 10). (H, I) IF staining was performed to evaluate the expression of *PCNA* in the tibial anterior muscle (n = 10). The analysis data are expressed as means ± SEM. $^{*}P < 0.05$ *vs* Vehicle group.

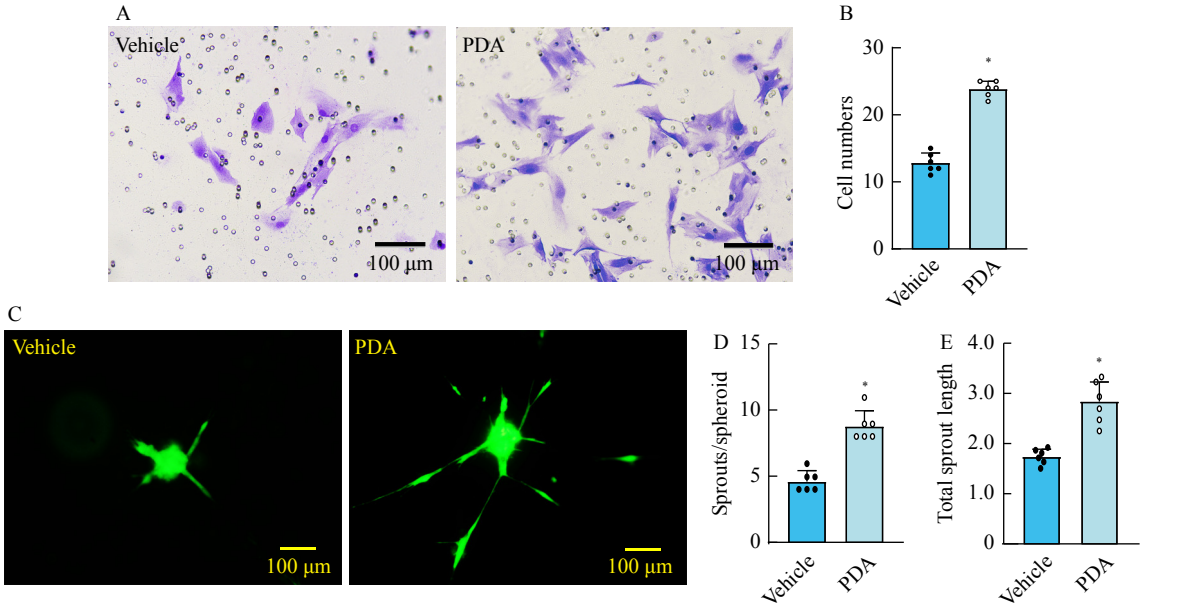

Fig. 3 PDA promotes the migration of rat SMCs. (A) Boyden chamber cell migration assay was performed in the presence of PDA (10 μmol·L^{-1}), and migrating cells were observed by crystal violet staining. The number of cells is shown in (B) (n = 6). (C) A spherical germination test was performed in the presence of PDA (10 μmol·L^{-1}), and germination of SMCs was observed by calcein-AM staining. Qquantitative analysis results of bud length and bud length are shown in (D, E) (n = 6). Data are expressed as mean ± SEM. $^{*}P < 0.05$ *vs* Vehicle group.

pression of *MyD88* in a time-dependent manner (3, 6, 12, 24, and 48 h), reaching a peak between 12 and 24 h (Figs. 4D and 4E). To determine the *in vivo* relevance of these findings, we performed IHC staining of *MyD88* on tissue sections from the complete ligation model of the left common carotid artery. The analysis revealed a basal expression of *MyD88* in the media smooth muscle layer and an induction in the neointima areas following vascular injury, further enhanced by 14 d of PDA treatment (Figs. 4F and 4G). After 21 d, PDA continued to increase *MyD88* expression in the neointima (Figs. 4H and 4I). Moreover, *MyD88* expression was also examined in a skeletal injury-induced angiogenesis model, where PDA treatment was found to promote *MyD88* expression in SMCs of newly formed vessels (Supplementary Figs. S10A−S10C). In summary, the data strongly suggest that PDA enhances *MyD88* expression in SMCs following vascular injury stimulation.

PDA promotes SMCs CDH13 expression following vascular injury stimulation

We next sought to determine whether PDA promotes *CDH13* expression. It was observed that PDA treatment notably increased the transcription of *CDH13* (Fig. 5A). Further analysis involved treating SMCs with varying concentrations of PDA (1, 5, 10, 15, and 20 μmol·L^{-1}) and evaluating *CDH13* expression through the Western blotting assay. Our results indicated that treatment with 5, 10, and 15 μmol·L^{-1} PDA dramatically promoted CDH13 protein levels (Figs. 5B and 5C). To evaluate the time-dependent effect of PDA on *CDH13* expression, we treated SMCs with 10 μmol·L^{-1} PDA and analyzed using the Western blotting assay at various time points (3, 6, 12, 24, and 48 h) treatment. The results indicated a substantial increase in *CDH13* expression at 6, 12, and 24 h post-treatment (Figs. 5D and 5E). The study further extended to *in vivo* models to confirm these findings. IHC staining of *CDH13* was performed on tissue sections from a left common carotid artery ligation model. The results showed that vascular injury itself increased *CDH13* expression, predominantly in the nucleus. Notably, 14 d of PDA treatment significantly augmented *CDH13* expression within the neointima area (Figs. 5F and 5G). This enhanced expression was also evident after 21 d of PDA treatment (Figs. 5H and 5I). Additionally, in a skeletal muscle injury-induced angiogenesis model, PDA treatment was found to significantly increase *CDH13* expression in the SMCs of newly formed vessels (Supplementary Figs. S11A−S11C). Our data indicate that PDA induces *CDH13* expression in SMCs following vascular injury.

PDA promotes pathological vascular remodeling by regulating the interaction between MyD88 and CDH13

Although both *MyD88* and *CDH13* are implicated in pathological vascular remodeling, the nature of their interaction remains unclear. In our animal studies, we sought to determine whether *MyD88* and *CDH13* co-express. Due to species-related antigenic limitations in IF staining, we employed a combination of IHC and IF staining to locate the expression of *MyD88* and *CDH13* within SMCs. The results revealed that *MyD88* and *CDH13* were expressed in SMCs in adjacent skeletal muscle sections (Fig. 6A, Supplementary Fig. S12), suggesting co-localization in the SMCs of the skeletal muscle. Further, a molecular docking simulation was conducted using AutoDock Vina 1.5.6 software to predict the interaction of PDA with *MyD88* and *CDH13*. The three-di-

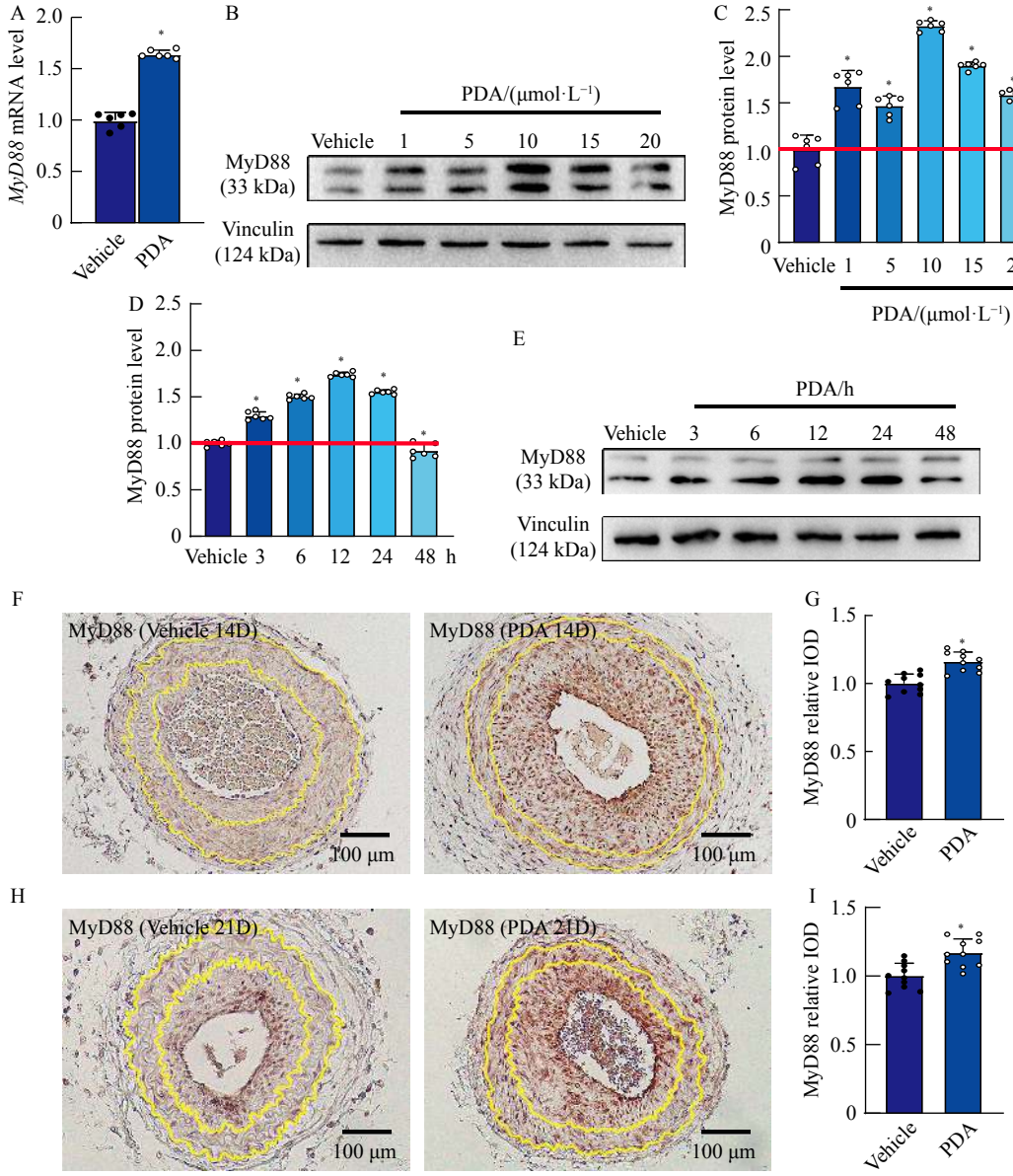

Fig. 4 PDA induces SMCs *MyD88* expression following vascular injury stimulation. (A) Rat SMCs treated with PDA (10 μmol·L^{-1}) for 24 h. Real-time PCR was performed to detect the mRNA level of the *MyD88* (n = 6). (B) SMCs were treated with different doses of PDA at 1, 5, 10, 15, and 20 μmol·L^{-1}, and the expression of MyD88 was detected by Western blotting. (C) Quantification of the relative protein level of MyD88 (n = 6). (D) Western blotting was used to detect the expression of MyD88 in SMCs after PDA (10 μmol·L^{-1}) treatment at different time points, and quantitative data are shown in (E) (n = 6). (F) IHC staining was used to detect the expression of MyD88 in the complete ligation model of the left common carotid artery on day 14. (G) Relative protein levels were quantified by mean optical density (integrated optical density/area) using Image J software (n = 10). (H) IHC staining was used to detect the expression of MyD88 in the complete ligation model of the left common carotid artery after 21 d of PDA treatment. (I) Relative protein levels were quantified by mean optical density (integrated optical density/area) using Image J software (n = 10). Data are expressed as mean ± SEM, $^*P < 0.05$ *vs* Vehicle group.

mensional structures of these proteins were sourced from the RCSB PDB database (http://www.rcsb.org/). This analysis revealed multiple potential binding sites of PDA with *MyD88* and *CDH13* (Fig. 6B). Binding energies less than zero were considered indicative of spontaneous binding and interaction, with −6.5 kcal·mol^{-1} observed for PDA-*MyD88* and −7.4 kcal·mol^{-1} for PDA-*CDH13* (Fig. 6C). To validate this hypothesis, we performed co-immunoprecipitation assay. Our data confirmed the interaction between *MyD88* and *CDH13 in vivo* (Fig. 6D). These findings support the notion that PDA may influence pathological vascular remodeling, at least in part, by modulating the interaction between *MyD88* and *CDH13*.

Inhibition of MyD88 attenuates PDA-induced pathological vascular remodeling

We suppressed *MyD88* in SMCs by TJ-M2010-5

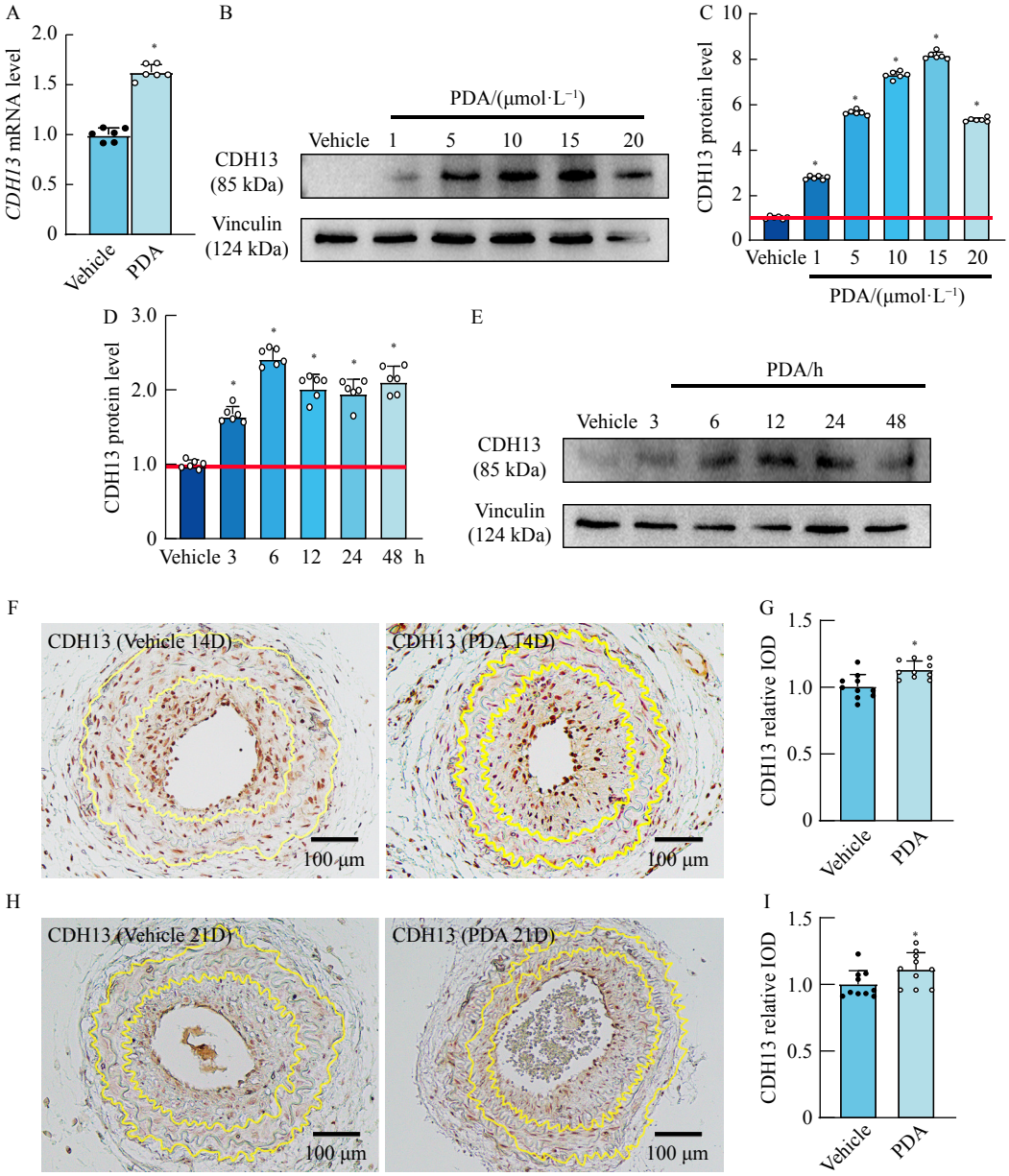

Fig. 5 PDA promotes *CDH13* expression in SMCs following vascular injury stimulation. (A) Rat SMCs treated with PDA (10 μmol·L^{-1}) for 24 h. Real-time PCR was performed to detect the mRNA level of the *CDH13* (n = 6). (B) SMCs were treated with different doses of PDA at 1, 5, 10, 15, and 20 μmol·L^{-1}, and the expression of CDH13 was detected by Western blotting. (C) Quantification of the relative protein level of CDH13 (n = 6). (D) Western blotting was used to detect the expression of CDH13 in SMCs after PDA (10 μmol·L^{-1}) treatment at different time points, and quantitative data are shown as (E) (n = 6). (F) IHC staining was used to detect the expression of CDH13 in the complete ligation model of the left common carotid artery on day 14. (G) Relative protein levels were quantified by mean optical density (integrated optical density/area) using Image J software (n = 10). (H) IHC staining was used to detect the expression of CDH13 in the complete ligation model of the left common carotid artery on day 21. (I) Relative protein levels were quantified by mean optical density (integrated optical density/area) using Image J software (n = 10). Data are expressed as mean ± SEM, $^*P < 0.05$ *vs* Vehicle group.

($C_{23}H_{26}N_4OS$, a *MyD88* inhibitor) treatment. Real-time PCR results analysis revealed that the transcription levels of *MyD88* and its downstream gene, *CDH13*, were significantly reduced following treatment with TJ-M2010-5 (Supplementary Figs. S13A and S13B). Inhibition of *MyD88* on other cell growth-related genes after PDA treatment was examined by real-time PCR (Supplementary Fig. 14). The results showed that PDA treatment increased BrdU incorporation in SMCs. However, this PDA-induced increase in BrdU incorporation was mitigated upon *MyD88* inhibition (Figs. 7A and 7B). PDA treatment facilitated cell migration, as assessed by the Boyden chamber migration assay. The inhibition of *MyD88* partially reversed the PDA-induced increase in cell migration (Figs. 7C and 7D). The increased numbers and lengths of cell

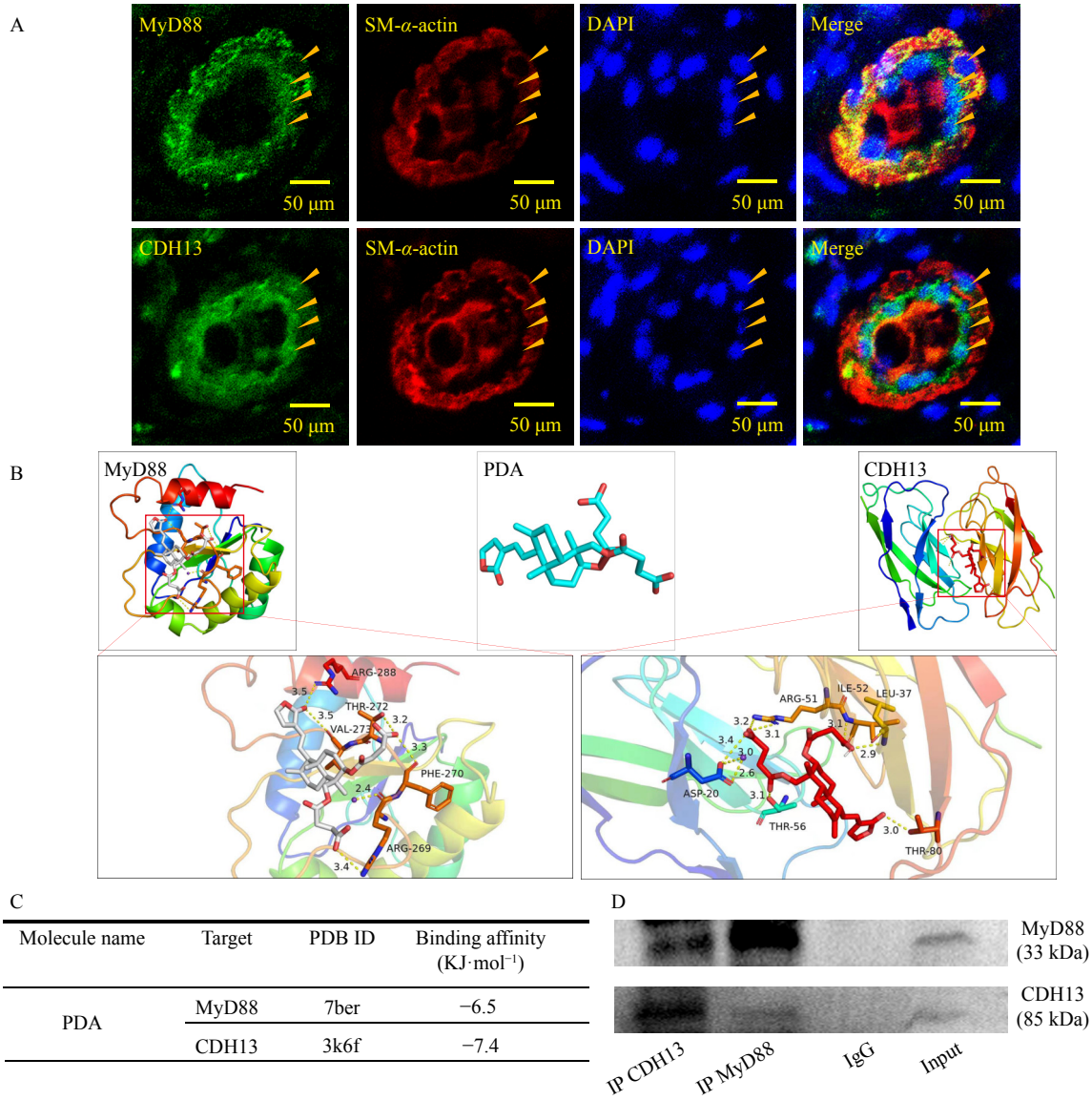

C

Molecule name	Target	PDB ID	Binding affinity (KJ·mol^{-1})
PDA	MyD88	7ber	−6.5
	CDH13	3k6f	−7.4

Fig. 6 PDA promotes pathological vascular remodeling by regulating the interaction between *MyD88* and *CDH13*. (A) IF staining of MyD88 and CDH13 was performed on adjacent tissue sections to assess the co-expression of these proteins in newly formed vascular SMCs. (B) A molecular docking simulation was performed to evaluate the binding energy of PDA with MyD88 and CDH13 using Autodock Vina 1.5.6 software developed by Olson's research group. In this simulation, PDA was set as the receptor, while MyD88 and CDH13 were treated as ligands. The three-dimensional structures of MyD88 and CDH13 were obtained from the RCSBPDB database (http://www.rcsb.org/). Binding energies less than zero indicated a propensity for spontaneous binding and interaction. (C) The specific binding energies obtained from the molecular docking simulation between PDA and MyD88 and between PDA and CDH13 (D) Co-immunoprecipitation was performed to determine the interaction between MyD88 and CDH13. Total protein was extracted from rat SMCs using RIPA buffer. The cell lysate was precleared using anti-species-specific IgG beads. The precleared cell lysate was incubated with MyD88 (Affinity) and CDH13 (Pro Sci) for 1 h at 4 °C. Following incubation with pre-equilibrated protein A/G agarose beads on a rocking platform overnight at 4 °C, the co-immunoprecipitated targets were evaluated by Western blotting.

sprouts induced by PDA treatment were also attenuated following *MyD88* inhibition (Figs. 7E−7G). These results collectively suggest that PDA promotes pathological vascular remodeling associated with SMCs, at least in part, through a mechanism involving *MyD88*.

In summary, PDA can increase SMCs *MyD88* expression. This increase leads to an interaction between *MyD88* and *CDH13*, which is pivotal in enhancing proliferation, migration, and extracellular matrix deposition, culminating in the progression of pathological vascular remodeling (Fig. 7H).

Discussion

This study elucidates the critical role of PDA in modulating pathological vascular remodeling. A key finding is the in-

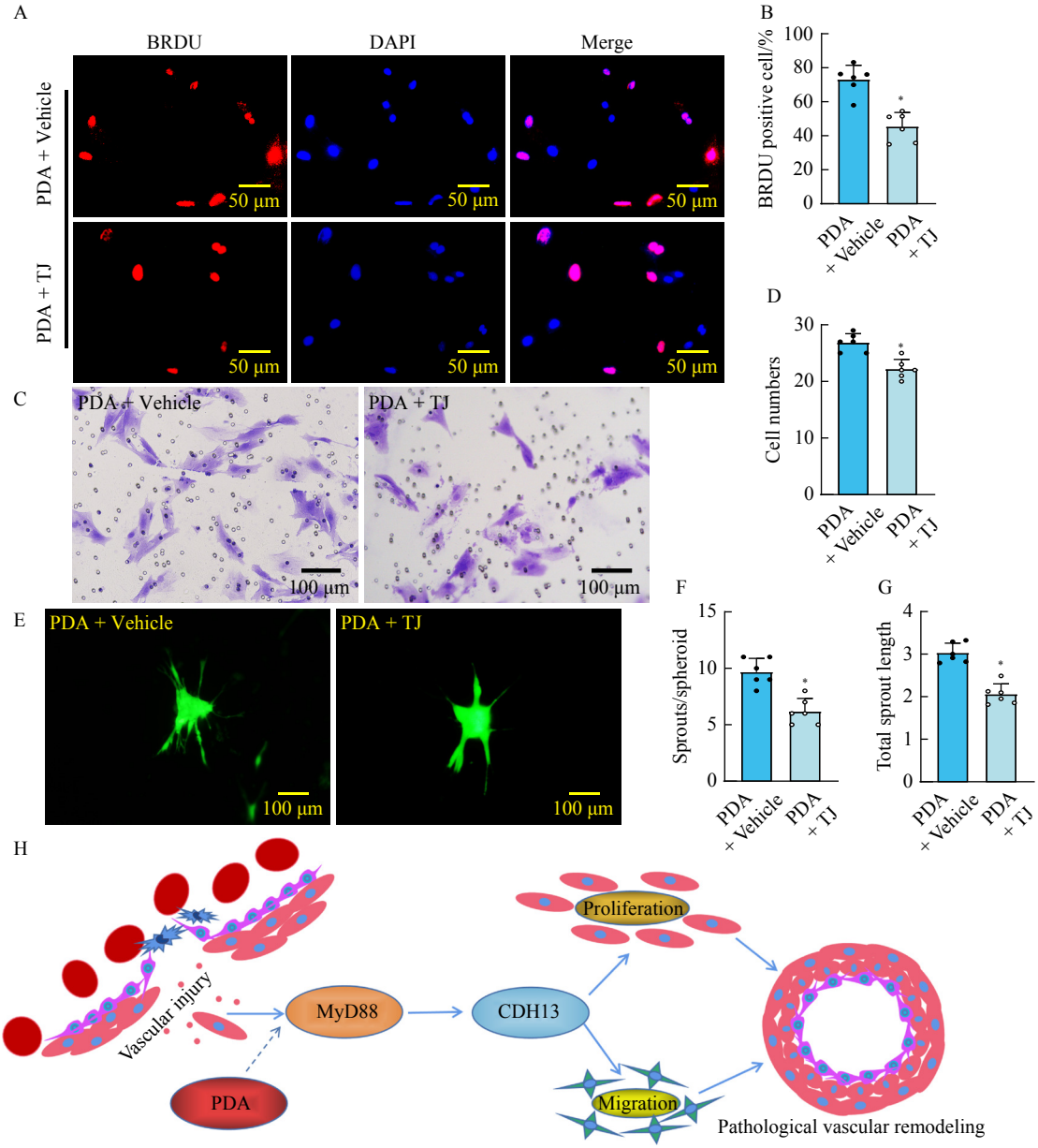

Fig. 7 Inhibition of *MyD88* attenuates PDA-induced pathological vascular remodeling. (A) Rat SMCs were treated with TJ-M2010-5 (10 μmol·L^{-1}) and PDA (10 μmol·L^{-1}), followed by incubation with BrdU labeling buffer for 20 h. IF staining was performed to observe BrdU incorporation, and BrdU-positive cells were quantified, as shown in (B). (C) A Boyden chamber cell migration assay was performed in the presence of TJ-M2010-5 (10 μmol·L^{-1}) and PDA (10 μmol·L^{-1}). Cell migration was visualized using crystal violet staining, and the number of migrating cells is displayed in (D) (n = 6). (E) A spheroid sprouting assay was performed in the presence of TJ-M2010-5 (10 μmol·L^{-1}) and PDA (10 μmol·L^{-1}). The sprouting was visualized by calcein-AM staining, and sprout number and length were quantified, as shown in (F, G) (n = 6). (H) A schematic diagram indicating that PDA regulates pathological vascular remodeling through the *MyD88/CDH13* signaling pathway-dependent proliferation and migration of SMCs. Data are expressed as mean ± SEM, $^{*}P < 0.05$ *vs* PDA + Vehicle group.

duction of *MyD88* expression in SMCs following vascular injury, which is significantly augmented by PDA treatment. This increased *MyD88* expression fosters interaction with *CDH13*, leading to enhanced proliferation and migration of SMCs, ultimately resulting in pathological vascular remodeling.

Andrographolide, the primary constituent of the traditional Chinese medicinal herb *Andrographis paniculata*, serves as the precursor for PDA. Clinically, PDA is used for treating inflammatory diseases triggered by viral infections. Our recent publication highlighted PDA's ability to activate vascular endothelial cells, promoting proliferation, migration, and macrophage infiltration. This activity is associated with the dysfunction of the vascular endothelial barrier, as observed in a partially ligated carotid artery model, and is exacerbated by PDA treatment [38]. However, the specific role of

PDA in promoting neointima formation *via* SMC phenotypic switching has not been previously reported. In this study, we demonstrate that PDA induces neointima formation, characterized by increased proliferation and migration of SMCs, in a complete ligation model of the left common carotid artery.

PDA's efficacy in treating respiratory virus-associated inflammatory diseases is well-known, yet the underlying mechanisms remain largely unexplored. Viral infection-induced inflammation is a dynamic process influenced by the immune system, the host, and the virus itself [39]. PDA exacerbates vascular inflammation in disturbed blood flow models, associated with endothelium barrier dysfunction and inflammatory cell infiltration. Notably, PDA treatment significantly promotes vascular neointima formation and appears to aid in endothelial barrier repair [38].

The relationship between vascular inflammation and SMC phenotypic switching is complex and not fully understood. Inflammation can occur at various stages of vascular diseases, such as atherosclerosis, aortic dissection, varicose veins, and aneurysms. These conditions involve multiple cell types and signaling pathways contributing to the inflammatory process.

SMC phenotypic switching, the transition from a differentiated to a dedifferentiated state, typically leads to vascular wall thickening and potential thrombogenesis or atherosclerosis. Interestingly, certain vascular diseases like varicose veins and aneurysms are characterized by a decrease in SMC numbers. Our study revealed that PDA promoted SMC proliferation and migration, leading to neointima formation, which may offer novel insights for diseases associated with reduced SMC numbers.

In conclusion, PDA's role in enhancing neointima formation through the regulation of SMC proliferation and migration presents a potential novel therapeutic strategy for vascular diseases characterized by decreased SMC numbers.

Supporting Information

Supporting information of this paper can be requested by sending E-mail to the corresponding author.

References

[1] Steffes LC, Froistad AA, Andruska A, *et al*. A notch3-marked subpopulation of vascular smooth muscle cells is the cell of origin for occlusive pulmonary vascular lesions [J]. *Circulation*, 2020, **142**(16): 1545-1561.

[2] Shi R, Babu S. Modern approaches and innovations in the diagnosis and treatment of peripheral vascular diseases [J]. *Front Biosci*, 2021, **13**(2): 173-180.

[3] Luo L, Cai Y, Zhang Y, *et al*. Role of PDE10A in vascular smooth muscle cell hyperplasia and pathological vascular remodelling [J]. *Cardiovasc Res*, 2022, **118**(12): 2703-2717.

[4] Rajendran P, Rengarajan T, Thangavel J, *et al*. The vascular endothelium and human diseases [J]. *Int J Biol Sci*, 2013, **9**(10): 1057-1069.

[5] Alexander MR, Owens GK. Epigenetic control of smooth muscle cell differentiation and phenotypic switching in vascular development and disease [J]. *Annu Rev Physiol*, 2012, **74**: 13-40.

[6] Davis GE, Senger DR. Endothelial extracellular matrix: biosynthesis, remodeling, and functions during vascular morphogenesis and neovessel stabilization [J]. *Circ Res*, 2005, **97**(11): 1093-1107.

[7] Ji QX, Zeng FY, Zhou J, *et al*. Ferroptotic stress facilitates smooth muscle cell dedifferentiation in arterial remodelling by disrupting mitochondrial homeostasis [J]. *Cell Death Differ*, 2023, **30**(2): 457-474.

[8] Jain M, Dhanesha N, Doddapattar P, *et al*. Smooth muscle cell-specific fibronectin-EDA mediates phenotypic switching and neointimal hyperplasia [J]. *J Clin Invest*, 2020, **130**(1): 295-314.

[9] Incalza MA, D'Oria R, Natalicchio A, *et al*. Oxidative stress and reactive oxygen species in endothelial dysfunction associated with cardiovascular and metabolic diseases [J]. *Vascul Pharmacol*, 2018, **100**: 1-19.

[10] Godo S, Shimokawa H. Endothelial functions [J]. *Arterioscler Thromb Vasc Biol*, 2017, **37**(9): e108-e114.

[11] Hsu PL, Chen JS, Wang CY, *et al*. Shear-induced CCN1 promotes atheroprone endothelial phenotypes and atherosclerosis [J]. *Circulation*, 2019, **139**(25): 2877-2891.

[12] Domingues A, Boisson-Vidal C, Marquet DRP, *et al*. Targeting endothelial thioredoxin-interacting protein (TXNIP) protects from metabolic disorder-related impairment of vascular function and post-ischemic revascularisation [J]. *Angiogenesis*, 2020, **23**(2): 249-264.

[13] Propson NE, Roy ER, Litvinchuk A, *et al*. Endothelial C3a receptor mediates vascular inflammation and blood-brain barrier permeability during aging [J]. *J Clin Invest*, 2021, **131**(1): e140966.

[14] Vanhoutte PM, Shimokawa H, Feletou M, *et al*. Endothelial dysfunction and vascular disease: a 30th anniversary update [J]. *Acta Physiol (Oxf)*, 2017, **219**(1): 22-96.

[15] Ran R, Cai D, King SD, *et al*. Surfactant protein A, a novel regulator for smooth muscle phenotypic modulation and vascular remodeling-brief report [J]. *Arterioscler Thromb Vasc Biol*, 2021, **41**(2): 808-814.

[16] Janssens S, Beyaert R. A universal role for MyD88 in TLR/IL-1R-mediated signaling [J]. *Trends Biochem Sci*, 2002, **27**(9): 474-482.

[17] Parpaleix A, Amsellem V, Houssaini A, *et al*. Role of interleukin-1 receptor 1/MyD88 signalling in the development and progression of pulmonary hypertension [J]. *Eur Respir J*, 2016, **48**(2): 470-483.

[18] Song Y, Shen H, Schenten D, *et al*. Aging enhances the basal production of IL-6 and CCL2 in vascular smooth muscle cells [J]. *Arterioscler Thromb Vasc Biol*, 2012, **32**(1): 103-109.

[19] Saxena A, Rauch U, Berg KE, *et al*. The vascular repair process after injury of the carotid artery is regulated by IL-1RI and MyD88 signalling [J]. *Cardiovasc Res*, 2011, **91**(2): 350-357.

[20] Engelbertsen D, Rattik S, Wigren M, *et al*. IL-1R and MyD88 signalling in CD4$^+$ T cells promote Th17 immunity and atherosclerosis [J]. *Cardiovasc Res*, 2018, **114**(1): 180-187.

[21] Shen H, Eguchi K, Kono N, *et al*. Saturated fatty acid palmitate aggravates neointima formation by promoting smooth muscle phenotypic modulation [J]. *Arterioscler Thromb Vasc Biol*, 2013, **33**(11): 2596-2607.

[22] Owens AP, Rateri DL, Howatt DA, *et al*. MyD88 deficiency attenuates angiotensin II-induced abdominal aortic aneurysm formation independent of signaling through Toll-like receptors 2 and 4 [J]. *Arterioscler Thromb Vasc Biol*, 2011, **31**(12): 2813-2819.

[23] Ivanov D, Philippova M, Antropova J, *et al*. Expression of cell adhesion molecule T-cadherin in the human vasculature [J].

Histochem Cell Biol, 2001, **115**(3): 231-242.

[24] Kudrjashova E, Bashtrikov P, Bochkov V, *et al*. Expression of adhesion molecule T-cadherin is increased during neointima formation in experimental restenosis [J]. *Histochem Cell Biol*, 2002, **118**(4): 281-290.

[25] Frismantiene A, Pfaff D, Frachet A, *et al*. Regulation of contractile signaling and matrix remodeling by T-cadherin in vascular smooth muscle cells: constitutive and insulin-dependent effects [J]. *Cell Signal*, 2014, **26**(9): 1897-1908.

[26] Takeuchi T, Adachi Y, Ohtsuki Y, *et al*. Adiponectin receptors, with special focus on the role of the third receptor, T-cadherin, in vascular disease [J]. *Med Mol Morphol*, 2007, **40**(3): 115-120.

[27] Rubina K, Talovskaya E, Cherenkov V, *et al*. LDL induces intracellular signalling and cell migration *via* atypical LDL-binding protein T-cadherin [J]. *Mol Cell Biochem*, 2005, **273**(1-2): 33-41.

[28] Kipmen-Korgun D, Osibow K, Zoratti C, *et al*. T-cadherin mediates low-density lipoprotein-initiated cell proliferation *via* the $Ca^{(2+)}$-tyrosine kinase-Erk1/2 pathway [J]. *J Cardiovasc Pharmacol*, 2005, **45**(5): 418-430.

[29] Hebbard LW, Garlatti M, Young LJ, *et al*. T-cadherin supports angiogenesis and adiponectin association with the vasculature in a mouse mammary tumor model [J]. *Cancer Res*, 2008, **68**(5): 1407-1416.

[30] Ivanov D, Philippova M, Allenspach R, *et al*. T-cadherin upregulation correlates with cell-cycle progression and promotes proliferation of vascular cells [J]. *Cardiovasc Res*, 2004, **64**(1): 132-143.

[31] Kyriakakis E, Frismantiene A, Dasen B, *et al*. T-cadherin promotes autophagy and survival in vascular smooth muscle cells through MEK1/2/Erk1/2 axis activation [J]. *Cell Signal*, 2017, **35**: 163-175.

[32] Fujishima Y, Maeda N, Matsuda K, *et al*. Adiponectin association with T-cadherin protects against neointima proliferation and atherosclerosis [J]. *FASEB J*, 2017, **31**(4): 1571-1583.

[33] Rubina K, Kalinina N, Potekhina A, *et al*. T-cadherin suppresses angiogenesis *in vivo* by inhibiting migration of endothelial cells [J]. *Angiogenesis*, 2007, **10**(3): 183-195.

[34] Yao H, Wu Z, Xu Y, *et al*. Andrographolide attenuates imbalance of gastric vascular homeostasis induced by ethanol through glycolysis pathway [J]. *Sci Rep*, 2019, **9**(1): 4968.

[35] Hu W, Wu X, Jin Z, *et al*. Andrographolide promotes interaction between endothelin-dependent EDNRA/EDNRB and myocardin-SRF to regulate pathological vascular remodeling [J]. *Front Cardiovasc Med*, 2021, **8**: 783872.

[36] Su L, Gao Y, Zhang M, *et al*. Andrographolide and its derivative potassium dehydrographolide succinate suppress PRRSV replication in primary and established cells *via* differential mechanisms of action [J]. *Virol Sin*, 2021, **36**(6): 1626-1643.

[37] Wang Y, Hu G, Liu F, *et al*. Deletion of yes-associated protein (YAP) specifically in cardiac and vascular smooth muscle cells reveals a crucial role for YAP in mouse cardiovascular development [J]. *Circ Res*, 2014, **114**(6): 957-965.

[38] Wang Z, Wu X, Li J, *et al*. Potassium dehydroandrograpolide succinate targets NRP1 mediated VEGFR2/VE-cadherin signaling pathway to promote endothelial barrier repair [J]. *Int J Mol Sci*, 2023, **24**(4): 3096.

[39] Sullivan C, Soos BL, Millard PJ, *et al*. Modeling virus-induced inflammation in zebrafish: a balance between infection control and excessive inflammation [J]. *Front Immunol*, 2021, **12**: 636623.

Cite this article as: GUO Qiru, LI Jiali, WANG Zheng, WU Xiao, JIN Zhong, ZHU Song, LI Hongfei, ZHANG Delai, HU Wangming, XU Huan, YANG Lan, SHI Liangqin, WANG Yong. Potassium dehydroandrographolide succinate regulates the *MyD88/CDH13* signaling pathway to enhance vascular injury-induced pathological vascular remodeling [J]. *Chin J Nat Med*, 2024, **22**(1): 62-74.